Femtosecond X-ray-induced fragmentation of fullerenes

N. Berrah[1], B. Murphy[2], H. Xiong[1], L. Fang[3], T. Osipov[4], E. Kukk[5], M. Guehr[6], R. Feifel[7], V. Petrovic[6], K. R. Ferguson[4,8], J. D. Bozek[4#], C. Bostedt[4], L. J. Frasinski[9], P. H. Bucksbaum[6] and J. C. Castagna[4]

[1]University of Connecticut, Physics Department, Storrs, CT 06269, USA
[2] Western Michigan University, Physics Department, Kalamazoo, MI 49008, USA
[3]University of Texas, Center of High Energy Density Science, Austin, TX 78712, USA
[4]LCLS, National Accelerator Laboratory, Menlo Park, CA 94025, USA
[5] University of Turku, Department of Physics and Astronomy, FI-20014 Turku, Finland
[6] Stanford University, PULSE Institute, Stanford CA 94305, USA
[7] University of Gothenborg, Physics Department, SE-412 96 Gothenburg, Sweden
[8]Department of Applied Physics, Stanford University, Stanford CA 94305, USA
[9] Imperial College London, Department of Physics, UK

(Feb 7, 2015)

Abstract

A new class of femtosecond, intense, short wavelength lasers − the free electron laser − has opened up new opportunities to investigate the structure and dynamics in many scientific areas. These new lasers, whose performance keeps increasing, enable the understanding of physical and chemical changes at an atomic spatial scale and on the time scale of atomic motion which is essential for a broad range of scientific fields. We describe here the interaction of fullerenes in the multiphoton regime with the Linac Coherent Light Source (LCLS) free electron laser at SLAC National Laboratory. In particular, we report on new data regarding the ionization of $Ho_3N@C_{80}$ molecules and compare the results with our prior C_{60} investigation of radiation damage induced by the LCLS pulses. We also discuss briefly the potential impact of newly available instrumentation to physical and chemical sciences when they are coupled with FELs as well as theoretical calculations and modeling.

Keywords: FEL, multi-photon, absorption, fullerene, Auger decay, radiation damage.

Introduction

Emerging photon technologies have enabled a new class of femtosecond lasers to join the ultrafast laser family, namely the vacuum ultraviolet (VUV) and x-ray free electron lasers (FELs) operating now at several sites around the world (*1-5*). They are new powerful femtosecond photonic tools, spanning a wide photon energy range, from the infra-red (IR) to the hard x-rays. One of the important attributes of these intense lasers is that they are tunable, enabling a wide class of experiments, from non-linear science (*6-29*) to time-resolved dynamics in physics and chemistry (*30, 31*). Technological advances in building short pulse lasers in the wavelength regime from the infra-red (IR) to the hard x-rays coupled with state-of-the-art instrumentation and theoretical modeling are contributing new insights to physical, chemical and biological sciences, especially when they are paired with theoretical calculations and modeling (*32-36*).

Ultrafast x-rays from FELs, like synchrotron radiation, have photon energies sufficient to access core and inner-shell electrons. They are therefore different from visible optical lasers because they enable inside-out multiphoton ionization. Short wavelength radiation can also be produced by table top femtosecond laser systems in the form of high harmonic generation (HHG) but the fluence in the hard x-ray regime is still weak compared to FELs (*37*). X-ray absorption enables element-specificity, or in other words, one can target specific atoms within molecules or clusters and select specific shells in those atoms (by fine tuning the photon energy to specific spectral regions) (*38, 39*). This capability allows charting photochemical reactions and bioprocesses with atomic spatial resolution and femtosecond temporal resolution. Furthermore, the core-shell ionization and Auger decay processes, which are dominant in FEL-based work, lead to multiply charged fragments that can be compared to strong-field optical and infrared laser cases. Thus, comparisons between FEL-based and intense IR laser findings enable synergy and engagement of scientists from different communities, invigorating progress in science.

The FEL-based research in gas phase systems impacts applications ranging from single-pulse imaging of biomolecules to high-energy density materials as demonstrated by several works (*11, 14, 15, 27, 29, 32, 33*). Coherent diffractive imaging at the atomic level requires very short, intense x-ray pulses delivered effectively by free electron lasers (FEL) to record the diffraction pattern from biological molecules before they explode due to massive Coulomb explosion (*32, 33, 40-42*). This bio-imaging has been demonstrated with resolution of tens of nanometers (*43*), but atomic resolution will require the understanding of ultrafast multiphoton ionization dynamics from inner shells which can be very well studied by atomic and molecular spectroscopic methodologies (*11, 14, 28, 30, 31*). The early FEL-based experiments provided insight on the nature of the interaction of light atoms such as Ne (*11*) and small molecules such as N_2 (*26*) with intense X-ray pulses. When conducting experiments with x-ray FEL, multi-photon ionization and subsequent Auger decay contribute substantially to what is called "electronic damage" (*11, 26*). This damage will deteriorate the scattering images, ultimately limiting the resolution. The earlier atomic and molecular radiation damage findings motivated in part our current work to carry out FEL-based research on intermediate size molecules such as the fullerenes because they can provide detailed information on the ionization and radiation damage mechanisms (*14, 16*) since their size, unlike atoms (*14*) or small diatomic molecule (*16*), is closer to bio-systems.

Recently, we established through work on buckminsterfullerene (C_{60}) (*14*) a number of advantages for studying this sample as a benchmark case for radiation damage when compared with isolated atoms (*6,13*) small molecules (*17-19, 21-26*) or van der Waals (vdW) clusters (*27-29*). The main reason is that C_{60} consists entirely of C-C bonds and that chemically it has representative bond lengths and damage processes compared to bio-systems. Furthermore, the investigation of this system is still very active because it is the basis for many novel materials such as graphene or carbon nanotubes and thus connects to many applied fields. The interaction of x-ray FELs with matter is still terra-incognita since these lasers are only about five years old. Furthermore, theoretical models of large molecular femtosecond dynamics under ultrafast and intense x-ray laser exposure are now available and need to be systematically tested. Our work on C_{60} (*14*) molecules interacting with intense x-ray pulses provided by the LCLS, revealed the influence of processes not previously reported. In particular, our joint theoretical and experimental work illustrated the successful use of classical mechanics to describe all moving particles in C_{60}, an approach that scales well to larger systems, for example, bio-molecules. Understanding in detail the interaction of bio-molecules with FELs is important because they are one of the poster children for the construction of FELs since they hold the promise of single molecule diffractive imaging.

From a fundamental point of view, the understanding of photo-initiated dynamics depends upon investigating the intertwined electronic and nuclear motion which may require theoretical models beyond the Born–Oppenheimer approximation and including electron correlation. The electronic structure must be understood because it determines the potential energy surfaces along which the nuclear motion evolves. This is very difficult, however, due to the different interactions and the large number of degrees

of freedom that must be considered in order to completely describe even the smallest molecule. However, Molecular Dynamics (MD) modeling can advance the understanding of molecular femtosecond dynamics as we demonstrated in our recent work (*14, 16*).

The need to understand intermediate size molecular dynamics induced by XFEL pulses motivated the present work in endohedral fullerene with a high Z atom because it is a model system for bio-molecules such as iron-storage protein ferritin (*44*). Endohedral fullerenes are also relevant to medical physics applications of encapsulated fullerenes (*45*). A fundamental understanding of the electronic structure and photo-initiated nuclear dynamics in these molecules can be achieved by probing relaxation channels and re-organizational dynamics of highly excited molecules. This will enable understanding of large organic molecules and carbon nanomaterials, important for optimizing their properties for use in molecular electronics and organic photovoltaics (*46*).

Our goal with the reported investigation is three-fold: First, we aim to investigate the nature of the interaction and response of a large molecule, $Ho_3N@C_{80}$, with femtosecond photon pulses in order to contribute to the understanding of fundamental interactions of femtosecond XFEL radiation with complex systems such as a caged molecule. Second, we attempt to shed some light onto the basic question of radiation damage and how the molecular structure changes upon intense femtosecond x-ray absorption. Third, we want to compare this new work to our prior C_{60} work (*14, 16*). We also discuss in this manuscript future dynamical investigations with recently emerging instrument technologies paired with ultrafast x-ray photons and modeling. Although our primary interest is of fundamental nature, our results impact matter under extreme conditions because this community interprets their data using fundamental atomic and molecular physics results (*15*).

Experimental methodology

The experiment was performed using the atomic, molecular, and optical instrument described in other works (*11, 26, 47*). In particular, we used for this experiment a velocity map imaging (VMI) spectrometer (*48*) for detecting the ions produced in the interaction of the molecules with the LCLS pulses. The $Ho_3N@C_{80}$ molecules were collimated and introduced into the vacuum through a heated oven source. The photon energy and pulse durations are given in the results section. The pulse energy quoted is a nominal value measured upstream from the beam line optics. This values is reduced by 65%–85% in the interaction region due to photon beam transport losses (*11, 23, 26*). The photon beam was focused by Kirkpatrick-Baez (KB) mirrors to an approximately 5µm×5µm spot in the interaction chamber. For this experiment the interaction region was downstream of the optimal XFEL beam focus, compared to our C_{60} work (*14*), by about 1m because an instrument was inserted in the beamline upstream from the interaction region. This resulted in a decrease of the photon fluence.

To extract the kinetic energy (KE) from the time-of-flight (TOF) data recorded with the VMI we used the following procedure. For different initial KE of a specific ion, the time response of the detector was simulated using the SIMION software. In these simulations, an isotropic spatial distribution was assumed. The resulting time responses at different energies were used as the base functions. The KE distribution is extracted using a genetic algorithm, which mimics the natural selection. A random set of KE distributions were generated and evaluated as the first generation simulation and the best fits were selected. Mutation and crossover were applied to generate the next generation KE distribution. This process is iterated and stops when the optimization is found in successive simulation generations. In the present study, the resulting KE distribution was slightly dependent on the initial distribution (*49*). The error bars of stand-alone peaks are one standard deviation. For those mixed peaks, the counts are obtained by fitting the mass spectrum with Gaussian functions at fixed position of the designated fragments. The error bars were obtained by shifting the mass spectrum by ±0.2, as estimated deviation of the peak positions. The value of 0.2 was obtained from the peak width of $Ho_3N@C_{80}^{5+}$ where the width of the peak is about 0.7.

Results

The dominant ionization mechanism with intense FEL is sequential multiphoton absorption as observed in several previous works on atoms, molecules and clusters (*6-29*). Multiple sequential inner-shell photoionization (P) and subsequent Auger decay (A) events, accompanied by secondary ionization processes, lead to highly charged ionic states of the target by the absorption of multiple photons from a single x-ray pulse. As the highly charged parent molecule begins to break up, it and its fragments absorb additional photons through several sequential photoionization–Auger (P–A) cycles, leading to highly charged fragment ions. These repeated P–A cycles do not occur in single-photon absorption with conventional synchrotron radiation sources. The experiment on $Ho_3N@C_{80}$ was carried out with 1530 eV. This photon energy was chosen to optimize ionization from the Ho 3d shell. In fact, the total Ho photoabsorption cross section at this photon energy is 1.5 Mb while the Ho 3d shell contributes 1.2 Mb (*50*). The pulse duration was set to 80 fs and the pulse energy was nominal 2.2 mJ giving approximately 6.7×10^{18} photon/cm^2 (*11, 26*).
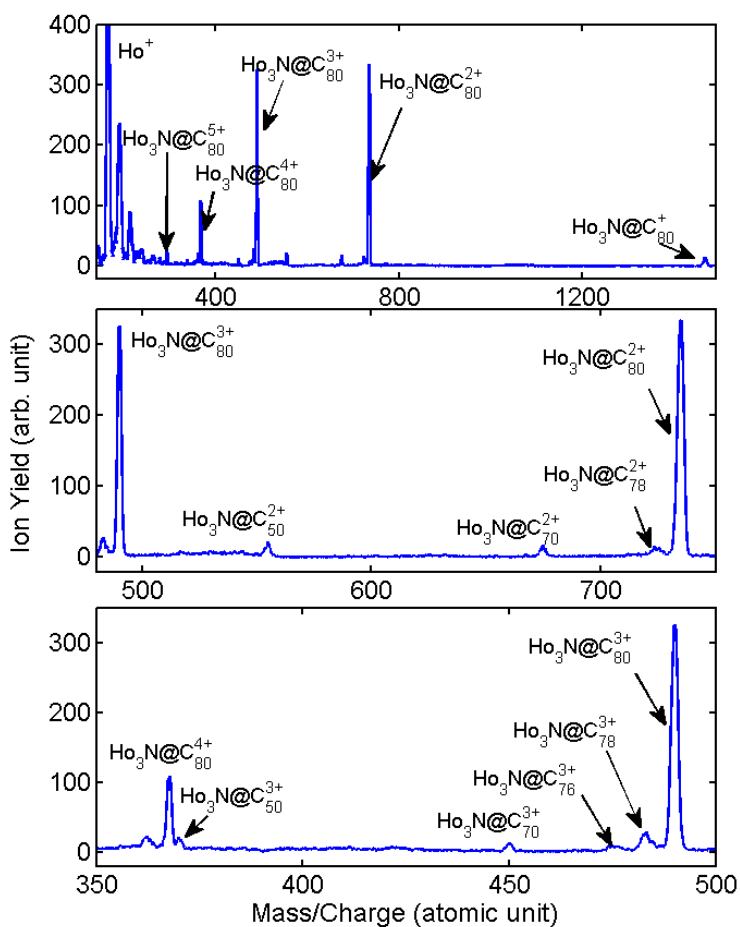
Fig. 1 Ion yield M/Q spectra displayed in three panels. The top panel displays all of the ion fragments while the middle and botton fragment focus on doubly and triply charged ions. (see text for details).

Fig. 1 shows signal attributed to multiphoton ionization processes for Ho_3N encapsulated into the fullerene $Ho_3N@C_{80}$. The three panels in Fig. 1 show the detected ions measured with the VMI

spectrometer. The top panel depicts peaks attributed to several multiply charged parent ions comprising singly charged $Ho_3N@C_{80}^+$ to quintuply charged $Ho_3N@C_{80}^{5+}$. We also observe the atomic Ho^+ ion which has the highest yield compared to all other ion fragments, originating from the fragmentation of the encapsulated Ho_3N molecule. The middle panel focuses on the doubly and triply ionized parent molecule along with doubly ionized fullerene molecules that lost C dimers such as $Ho_3N@C_{78}^{2+}$, $Ho_3N@C_{70}^{2+}$ and $Ho_3N@C_{50}^{2+}$; the loss of C dimers was also observed before with table-top experiments (46). The bottom panel shows the triply and quadruply charged parent molecules along with triply ionized parent molecules that lost C dimers, namely $Ho_3N@C_{78}^{3+}$, $Ho_3N@C_{76}^{3+}$, $Ho_3N@C_{70}^{3+}$, and $Ho_3N@C_{50}^{3+}$.
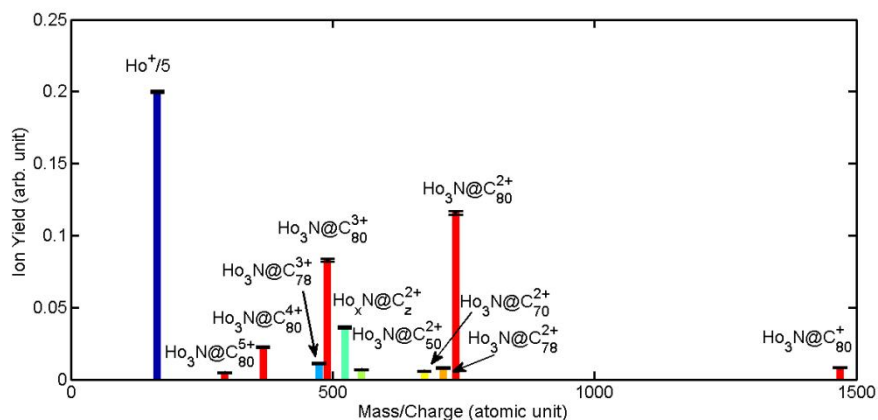

Fig. 2 All ion yield fragments are displayed. We used different colors for the parent, atomic and molecular fragment ions. (See text for details).

Fig. 2 displays all of the measured fragment ions in one panel for ease of visualizing the ion yield of each fragment. The different colors correspond to different ion fragments labelled in the figures. As can be seen in Fig. 2 the dominant ion yields are Ho^+ and the doubly and triply charged parent ions. The $Ho_xN@C_z^{2+}$ yield is in fact the sum of the fragments between $Ho_3N@C_{80}^{2+}$ and $Ho_3N@C_{50}^{3+}$ since they are not distinguishable in our experiment. We observe around the Ho^+ fragment ion a sea of singly charged molecular carbon fragment ions as shown in Fig. 3. We observe from the C_2^+ to C_{15}^+ as well as weak indication of doubly and triply charged Holmium atoms, Ho^{2+} and Ho^{3+}, embedded into the singly charged carbon ion fragments. It is worth noting that the largest observed molecular carbon fragment is C_{24}^+, although we only measure a weak amount of it.
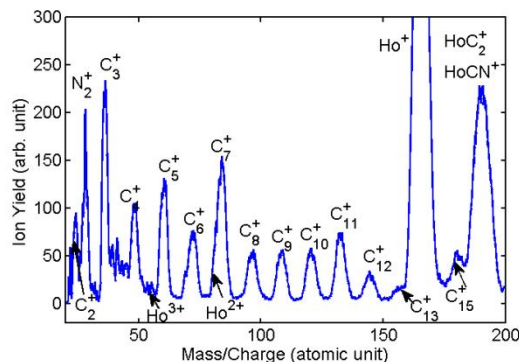
Fig. 3 Ion yield displaying the molecular ion fragments and focusing on the Carbon molecular ion fragments (see text for details).
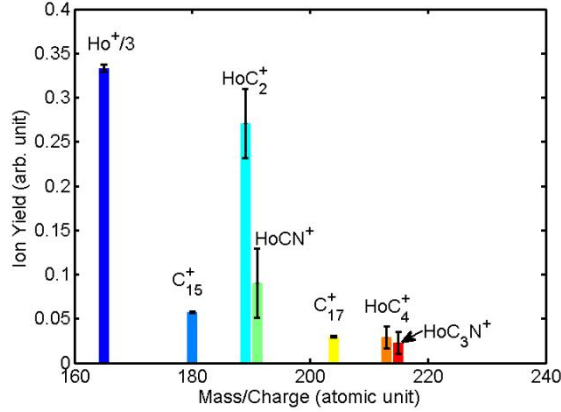
Fig. 4 Ion yield focusing on the atomic Ho ion and the Ho-based molecular ion fragments. (See text for details)

In order to spot other ion fragments we focus in Fig. 4 on the MASS/Q between 160 and 240 and find the following Ho-based molecular fragments: HoC_2^+, $HoCN^+$, HoC_3N^+ and HoC_4^+ along with the C ion fragment. Table 1 shows the branching ratios of the observed ion fragments with respect to the dominant Ho^+ ion which is singly charged atomic Ho^+. The next highest ion yields after Ho^+ are HoC_2^+ and $HoCN^+$.

**Table 1** Normalized branch ratios (%) of selected ion fragments.

Ho^+	Ho^{2+}	$Ho_3N@C_{80}^+$	$Ho_3N@C_{80}^{2+}$	$Ho_3N@C_{80}^{3+}$	$Ho_3N@C_{80}^{4+}$	$Ho_3N@C_{80}^{5+}$
100	4.8	0.83	12	8.3	2.3	0.47
C^+	C^{2+}	C^{3+}	HoC_2^+	$HoCN^+$	HoC_4^+	HoC_3N^+
53	12	0.53	27	9.0	2.9	2.3

The fragmentation dynamics of $Ho_3N@C_{80}$ also includes atomic C ion fragment shown in Fig. 5 where we observe C^+, C^{2+} and a very small amount of C^{3+}. This is unlike the case of the multiphoton ionization of C_{60} at 485 eV where for similar pulse duration (60 fs) the PAP sequence allowed the formation of up to C^{5+} (*14*). We note that at the photon energy of 485 eV used in the C_{60} investigation, the photo-absorption cross-section of carbon is 0.3 Mb which is much larger than 0.013 Mb at 1530 eV used in the present study. Thus, it is not surprising to only observe up to C^{3+}.
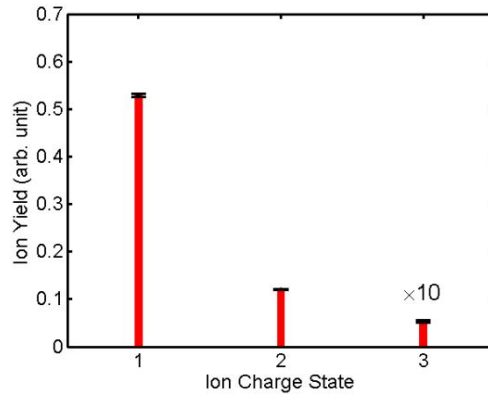
Fig. 5 Carbon ion yield for the charge states of C^+ to C^{3+}.

In order to understand the fragmentation dynamics and the KE sharing we analyzed the data as described above in the experimental section and plotted the kinetic energies in Fig. 6, along with the error bars of the C ion fragments. It appears that C^{2+} has a greater KE than C^+ as observed in our earlier work on C_{60} (*14*).
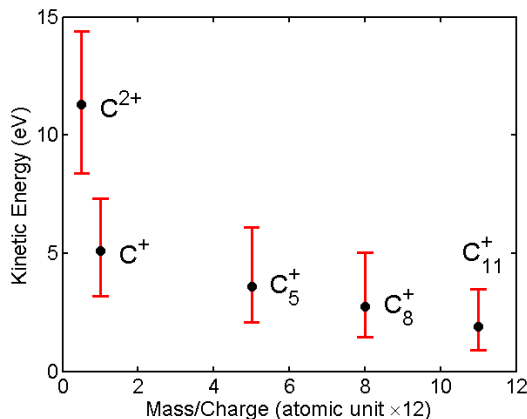
Fig. 6 Kinetic energy for selected atomic and molecular C fragments (see text for details).

We also find that the KE of singly charged carbon molecular fragments are similar to the KE of C^+. In order to understand where the deposited x-FEL pulse energy was transferred, we list in table 2 the C and Ho fragment ion KEs along with their error bars which is large for Ho^{2+} (since it is close to the C^{7+} ion fragment as shown in Fig.3). We fit the Ho^{2+} fragment to isolate it from C^{7+}, which results in a higher uncertainly.

**Table 2** Kinetic energy (KE) of C and Ho atomic ion fragments.

	C^+	C^{2+}	Ho^+	Ho^{2+}
KE (eV) (average value)	5.1	11.3	2.0	5.3
Upper deviation (eV)	2.2	3.1	1.3	4.7
Lower deviation (eV)	1.9	2.9	0.9	2.9

Since carbon ions are lighter than Ho ions, it is not surprising that their KE are larger than the Ho ions. The C KE are however much lower, about 10 eV for C^{2+} in the present work compared to 200 eV in the C_{60} work (14).

We present next our data with a different technique, namely covariance mapping. It is similar to ion-ion coincidence mapping which connects different fragments from individual dissociation events (39,48). However, in experiments where intense lasers are employed, many ions and electrons can be created in a single shot leading to false coincidences, requiring special correction techniques. Furthermore, ion-ion coincidence technique is not practical with the low FEL repetition rate of 120 Hz. A good alternative to ion-ion coincidence is covariance mapping, where the overabundance of ions per laser pulse is much less of a problem.

To extract the correlation in such experiments, the covariance map is used to clean out false correlation in high fluence mode (6, 51). In practice, ions from a single shot are considered as a row vector **X(t)**. The vector is also transposed to a column vector copy, $\mathbf{Y} = \mathbf{X}^T$. The covariance map is obtained by **cov<X,Y>** = **<X×Y>-1.1×<X><Y>** (51), where **<X×Y>** is the ion correlation average in single shot of all the FEL shots and **<X><Y>** is the product of averaged ion yields **<X>** and **<Y>**. For practical reason, the

background suppression is enhanced by subtracting 110% of the correlation, and the diagonal line is removed for better visibility of the correlation islands.
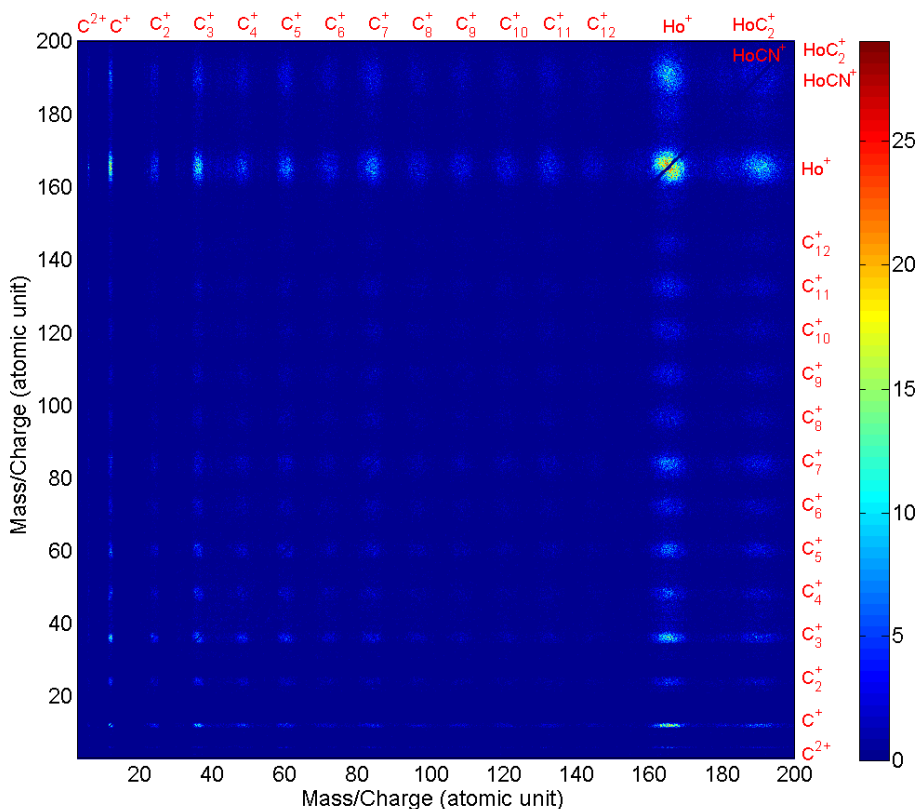
Fig. 7 Mass/charge covariance map of the fragments resulting from the Coulomb explosion of $Ho_3N@C_{80}$.

Fig. 7 shows the covariance map of the ion fragments resulting from the Coulomb explosion of $Ho_3N@C_{80}$ absorbing photons from the FEL. As we mentioned before, multiphoton absorption by Ho 3d electrons leads to a highly charged parent molecule. Similarly to C_{60}, the positive charge will be distributed evenly (52) on the cage after the core vacancies are filled. Since the carbon cage is highly charged, many ionic carbon fragments are created in a single explosion. Thus, correlation islands of most fragment pairs are observed.

The left panel of Fig. 8 presents the covariance map of small carbon fragments C_2^+ and C_3^+. A two-body Coulomb explosion would produce ions with perfectly correlated momenta and it would be seen as a tilted line (TOF-2 vs. TOF-1) in the covariance map. If more charges and atoms are involved in the Coulomb explosion, the correlation island would be characterized by a similar slope but a broadened shape because of the momentum carried away by other fragments (48). Total loss of correlation would result in a rectangular shaped covariance islands. Under the present experimental conditions, many bonds are broken in a single Coulomb explosion. Therefore the correlations between the individual small carbon ionic fragments are lost, resulting in rectangular patterns.

Discussion

The x-ray laser parameters for the interaction of $Ho_3N@C_{80}$ are different compared to the C_{60} work carried out with strong-fluence (*14*) and mid-fluence (*16*) regime. As mentioned above, the laser focus

8

was weaker due to the longer path the photons had to take to reach the interaction region. In fact, we estimate that the fluence used in the $Ho_3N@C_{80}$ is only ¼ of the fluence used in C_{60} (*14*), resulting in only a few multiphoton ionization cycles. This estimate is supported by our data since the intensity of the peaks of the highest charge states Ho^{2+} and C^{3+}, is very little, as shown in Fig. 5, compared to C^{5+} at comparable pulse duration in our previous C_{60} work (*14*).
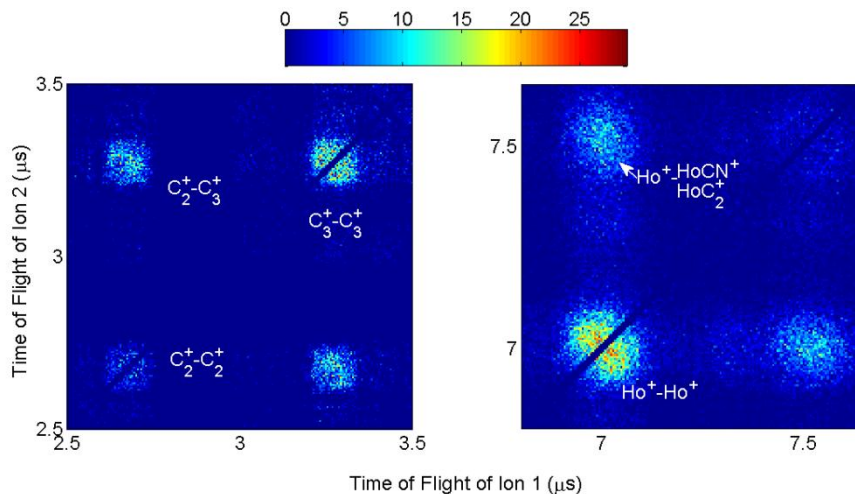
Fig. 8 Time of flight covariance map of small molecular fragments C_2^+ and C_3^+ (left panel) and Holmium-containing internal fragments (right panel).

In the C_{60} work we estimated 180 photons absorbed per C_{60} molecule while we estimate only 8 photons absorbed by $Ho_3N@C_{80}$. This implies that in the present work were in the low-fluence regime, where we can study the onset of fragmentation at relatively low total ion charge. Based on the absorption cross section of Ho (1.55 Mb) and C (0.013 Mb) at 1530 eV, we further estimate that Ho atoms absorbs 6 photons while the C cage absorbs 2 photons in the ionization of $Ho_3N@C_{80}$. The multiphoton absorption and Auger decay cascade in Ho lead then to multiply charges. Since we do not see any evidence of highly charged atomic Ho fragments, we are led to conclude that each Ho atoms may pull 6 electrons from the carbon cage to fill their vacancies, leading to highly charged C_{80}. Based on these estimates, our interpretation of the interaction of $Ho_3N@C_{80}$ with 1530 eV photon energy and with about $6.7 \cdot 10^{18}$ photons/cm^2 (compared to about $5 \cdot 10^{19}$ photons/cm^2 for the C_{60} experiment (*16*)) is that the parent molecule charges up and reaches at least $Ho_3N@C_{80}{}^{5+}$ as observed in Figs. 1&2. Since the Ho atoms are about ten times heavier than C atoms, we assume that they will not move faster than the carbon cage. We believe that as the carbon cage charges up, it will become unstable and fall apart leading to molecular fragments as shown in Fig. 3&4. This may be followed by the breakup of 3 Ho atoms, due to excited state repulsion.

Fig. 8 shows the Ho-containing ion fragments which are predominantly singly charged. On the other hand, Ho atom in an intact, neutral $Ho_3N@C_{80}$ cage has the oxidation number of +3 (53). From a simplified ionic point of view, each Ho in $Ho_3N@C80$ transfer 2 electrons to the C_{80} cage and one electron to N, completely filling the C_{80} HOMO cage and N valence shell. Thus, although the initial absorption favors even more positive charge creation at the Ho sites, during the charge redistribution and early dissociation stages, negative charge may flow into the Ho sites. Since the fragmentation of the cage occurs mostly as light fragments, and the heavier interior fragments have low charges, one can make a simple assumption that the explosion of the cage is a faster process that has little effect on the motion of the internal fragments from the viewpoint of the long-range Coulomb repulsion between fragments. In

order to model reliably the fragmentation dynamics, charge transfer dynamics must be modelled first. With the absence of such modelling, only some crude interpretation and predictions can be made.

The final average kinetic energy of Ho^+ is 2.0 eV. This can be compared, as a rough estimate, to the energy release from the explosion of a triangular planar configuration of three Ho^+ ions surrounding a central N atom (54). If we consider the Ho-N distance to be 2.1Å, based on prior work (55) and if we consider N as a neutral atom, the kinetic energy released per fragment will be 4.0 eV. However, as mentioned above, for accurate results charge migration dynamics must the known.

Note that the kinetic energy distribution of Ho^+, as seen in the right panel of Fig 8, is broad. We assume that this is the result of the fragmentation dynamics between the three Ho^+ atomic ions and the N atom surrounded by the carbon cage. Similar to a polyatomic molecule, the correlation of Ho^+- Ho^+ ion pair is observed to be broad and clearly tilted, as shown in the right panel of Fig. 8. Interestingly, similar correlation is not observed in Ho^+-(HoC_2^+, $HoCN^+$). It is speculated that the involvement of the Ho atoms in the carbon cage dissociation destroys such correlation.

Additional fragmentation mechanism occurs either in parallel or simultaneously because we observe in Figs. 1 and 2 the parent molecule multiply ionized, having lost C atoms since we observe $Ho_3N@C_m^{n+}$; n= 2,3 and m= 78, 76, 70 and 50. These weak fragments most probably lost C dimers as in previous intense IR work (*46*). We also observe weak mixed molecular fragment indicating that the Ho atom formed carbon and nitrogen bonds since we observe $HoCN^+$, HoC_2^+, HoC_4^+, HoC_3N^+ albeit in small quantity as can be seen in Fig. 4. Table 1 lists the branching rations between Ho ion and some carbon and molecular fragments.

Finally, inspired by the work on C_{60}, we plan in the future to investigate the ionization mechanisms of $Ho_3N@C_{80}$ at high fluence as in the case of C_{60} (*14*) and compare the results to MD models which are not yet available. We hope that our work the will further guide the development of molecular dynamics simulations suitable for even larger molecules exposed to intense XFEL pulses

Future research opportunities with emerging instrument technologies.

Femtosecond optical laser pulses have led to the development of transition state spectroscopy and femtosecond chemistry (*56*), and have been applied in pump-probe experiments to map out time-dependent nuclear motion in molecules (*57*). Similar schemes using optical laser and x-rays are being used with accelerator-based FELs (*30, 31, 58*) which are complementary to table-top optical lasers offering the opportunity to interrogate molecular dynamics in a site-specific manner. Furthermore, x-ray FEL-based research have already started to pursue femtosecond time-resolved experiments on bond-breaking in real time using x-ray pump x-ray probe experiments(59,60). One scheme is to use the soft x-ray split-and-delay (XRSD) instrument at the AMO Hutch (*61*). We plan to carry out time-resolved measurements on C_{60} at strong fluence for which the AMO hutch of the ALS is optimized for these types of measurements. We will use 10 fs pulse duration to conduct a virtually 'jitter-free' experiment tracking the ionization and fragmentation evolution of C_{60}. We will ionize the C cage with the first pulse and we will probe the dissociating molecules with the delayed second x-ray pulse. Our work in C_{60} predicted (*14, 16*) that the ionization dynamics occurs within the first few fs and remains into the ps regime. Such time-resolved information will be valuable in understanding the temporal development of radiation damage of medium size molecules such as C_{60}.

The past five years have been exciting with X-FEL-based experiments and the future holds many promises with the new FELs under construction around the world. Future FEL facilities are taking advantage of advances in focusing capabilities (*62*) and peak brightness to promise an even more robust regime of multiple photons absorbed per atom. In addition these new facilities will provide high repetition rate which will allow coincidence experiments (*63*). Furthermore, the pulse duration is planned to be even

shorter than a few femtoseconds (*64*), and the bandwidth narrower thanks to laser or self-seeding schemes (*65*) allowing routine pump-probe experiments to investigate electronic and nuclear dynamics. One can also foresee that time-resolved studies with sub-fs resolution: relying on attosecond x-ray pulses at intense FELs sources will be possible using x-ray split and delay devices (*56, 66, 67*) enabling scientists to measure in real time the electron dynamics and extract the timing of many fundamental ionization processes. Understanding the dynamics with atomic resolution and attosecond time structure will be revolutionary, enabling unanticipated discoveries.

Acknowledgements

Current address: SOLEIL synchrotron radiation facility, L'Orme des Merisiers Saint-Aubin - BP 48 91192 Gif-sur-Yvette, France.

References

(1) Berrah, N.; Bucksbaum, P.H. *Scientific American* **2014**, *310*, 64.

(2) Ackermann, W.; Asova, G.; Ayvazyan, V.; Azima, A.; Baboi, N.; Bähr, J.; Balandin, V.; Beutner, B.; Brandt, A.; Bolzmann, A.; et al. *Nature Photonics*, **2007**, *1,* 336 – 342.

(3) Emma, P.; Akre, R.; Arthur, J.; Bionta, R.; Bostedt, C.; Bozek, J.; Brachmann, A.; Bucksbaum, P.; Coffee, R.; Decker, F. J.; et al. *Nature Photonics* **2010**, *4,* 641 – 647.

(4) Allaria, E.; Appio, R.; Badano, L.; Barletta, W.A.; Bassanese, S.; Biedron, S.G.; Borga, A.; Busetto, E.; Castronovo, D.; Cinquegrana,, P.; et al. *Nature Photonics* **2012**, *6,* 699–704.

(5) Ishikawa, T.; Aoyagi, H.; Asaka, T.; Asano, Y.; Azumi, N.; Bizen, T.; Ego, H.; Fukami, K.; Fukui, T.; Furukawa, Y.; et al. *Nature Photonics* **2012**, *6,* 540–544.

(6) Frasinski, L.J.; Zhaunerchyk, V.; Mucke, M.; Squipp, R.J.; Siano, M.; Eland, J.H.D.; Linusson, P.; Meulen, P.v.d.; Salén, P.; R.D. Thomas, R.D.; et al. *Phys. Rev. Lett.* **2013**, *111,* 073002

(7) Bucksbaum, P.H.; Coffee, R.; Berrah, N., *Advances in Atomic, Molecular, and Optical Physics; Elsevier Inc.,* 2011; Chapter 60, p. 240.

(8) Kanter, E.P.; Krassig, B.; Li, Y.; March, A.M.; Rohringer, N.; Santra, R.; Southworth, S.H.; DiMauro, L.F.; Doumy, G.; Roedig, C.A.; et al. *Phys. Rev. Lett.* **2011**, *107*, 233001.

(9) Doumy, G.; Roedig, C.; Son, S.-K.; Blaga, C.I.; DiChiara, A.D.; Santra, R.; Berrah, N.; Bostedt, C.; Bozek, J.D.; Bucksbaum, P.H.; et al. *Phys. Rev. Lett.* **2011**, *106*, 083002.

(10) Berrah, N.; Bozek, J.; Costello, J.T.; Düsterer, S.; Fang, L.; Feldhaus, J.; Fukuzawa, H.; Hoener, M.; Jiang, Y.H.; Johnsson, P.; et al. *Journal of Modern Optics, Topical Review,* **2010**, *57,* (12) 1015-1040.

(11) Young, L.; Kanter, E.P.; Krässig, B.; Li, Y.; March, A.M.; Pratt, S.T.; Santra, R.; Southworth, S.H.; Rohringer, N.; DiMauro, L.F.; et al. *Nature* **2010**, *466*, 56-61.

(12) Rudek, B.; Son, S.K.; Foucar, L.; Epp, S.W.; Erk, B.; Hartmann, R.; Adolph, M.; Andritschke, R.; Aquila, A.; Berrah, N.; et al. *Nature Photonics* **2012**, *6,* 865.

(13) Erk, B.; Boll, R.; Trippel, S.; Anielski, D.; Foucar, L.; Rudek, B.; Epp, S.W.; Coffee, R.; Carron, S.; Schorb, S.; et al. *Science* **2014** *345* (6194), 288-291.

(14) Murphy, B.F.; Osipov, T.; Jurek, Z.; Fang, L.; Son S.-K.; Avaldi, L.; Bolognesi, P.; Bostedt, C.; Bozek, J.; Coffee, R.; et al. *Nature Comm,* **2014**, *5*, 4281.

(15) Vinko, S.M.; Ciricosta, O.; Cho, B.I.; Engelhorn, K.; Chung, H.K.; Brown, C.R.D.; Burian, T.; Chalupský, J.; Falcone, R.W.; Graves, C.; et al. *Nature* **2012**, *482*, 59–62.

(16) Berrah, N.; Fang, L.; Osipov, T.; Jurek, Z.; Murphy, B.F.; Santra, R.; *Faraday Disc.,* **2014**, *171 (1),* 471 – 485.

(17) Fang, L.; Rolles, D.; Rudenko, A.; Petrovich, V.; Bostedt, C.; Bozek, J.D.; Buckbaum, P; Berrah, N. *J. Phys. B: At. Mol. Opt. Phys.* **2014**, *47,* 124006.

(18) Berrah, N.; Fang, L.; Osipov, T.; Murphy, B.; Bostedt, C.; Bozek, J.D. *J. Elec. Spect and Rela. Phen,* **2014**, *196,* 34-37.

(19) Fang, L.; Osipov, T.; Murphy, B.; Tarantelli, F.; Kukk, E.; Cryan, J.P.; Glownia, M.; Bucksbaum, P.H.; Coffee, R.N.; Chen, M.; et al. *Phys. Rev. Lett.* **2012**, *109*, 263001.

(20) Murphy, B.F.; Fang, L.; Chen, M.H.; Bozek, J.D.; Kukk, E.; Kanter, E.P.; Messerschmidt, M.; Osipov, T.; Berrah, N. *Phys. Rev. A* **2012**, *86,* 053423.

(21) Salen, P.; Meulen, P.v.d.; Schmidt, H.T.; Thomas, R.D.; Larsson, M.; Feifel, R.; Piancastelli, M.N.; Fang, L.; Murphy, B.; Osipov, T.; et al. *Phys. Rev. Lett. PRL* **2012**, *108*, 153003.

(22) Osipov, T.Y.; Fang, L.; Murphy, B.F.; Hoener, M.; Berrah, N. *Journal of Physics: Conference Series* **2012**, *388*, 012030.

(23) Berrah, N.; Fang, L.; Osipov, T.; Murphy, B.; Kukk, E.; Ueda, K.; Feifel, R.; Meulen, P.v.d.; Salen, P.; Schmidt, H. et al. *Proc. Natl. Acad. Sci. USA(PNAS)* **2011**, *108, issue 41,* 16912.

(24) Cryan, J.P.; Glownia, J.M.; Andreasson, J.; Belkacem, A.; Berrah, N.; Blaga, C.I.; Bostedt, C.; Bozek, J.; Buth, C.; DiMauro, L.F. et al. *Phys. Rev. Lett* **2010**, *105,* 083004.

(25) Fang, L.; Hoener, M.; Gessner, O.; Tarantelli, F.; Pratt, S.T.; Kornilov, O.; Buth, C.; Guehr, M.; Kanter, E.P.; Bostedt, C.; et al. *Phys. Rev. Lett* **2010**, *105,* 083005.

(26) Hoener, M.; Fang, L.; Kornilov, O.; Gessner, O.; Pratt, S.T.; Guehr, M.; Kanter, E.P.; Blaga, C.; Bostedt, C.; Bozek, J.D. et al. *Phys. Rev. Lett.* **2010**, *104,* 253002.

(27) Bostedt, C.; Eremina, E.; Rupp, D.; Adolph, M.; Thomas, H.; Hoener, M.; Castro, A.R.B.d.; Tiggesbäumker, J.; Meiwes-Broer, K.-H.; Laarmann, T. et al, *Phys. Rev. Lett.* **2012**, *108*, 093401.

(28) Bostedt, C.; Adolph, M.; Eremina, E.; Hoener, M.; Rupp, D.; Schorb, S.; Thomas, H.; de Castro, A.R.B.; Möller, T. *J. Phys. B: At. Mol. Opt. Phys.* **2010**, *43*, 194011.

(29) Thomas, H.; Helal, A.; Hoffmann, K.; Kandadai, N.; Keto, J.; Andreasson, J.; Iwan, B.; Seibert, M.; Timneanu, N.; Hajdu, J. et al. *Phys. Rev. Lett.* **2012**, *108,* 133401.

(30) Petrović, V.S.; Siano, M.; White, J.L.; Berrah, N.; Bostedt, C.; Bozek, J.D.; Broege, D.; Chalfin, M.; Coffee, R.N.; Cryan, J. et al. *Phys. Rev. Lett.* **2012**, *108,* 253006.

(31) McFarland, B.K.; Farrell, J.P.; Miyabe, S.; Tarantelli, F.; Aguilar, A.; Berrah, N.; Bostedt, C.; Bozek, J.; Bucksbaum, P.H.; Castagna, J.C. et al. *Nat. Comm. 5* **2014**, 4235.

(32) Neutze, R.; Wouts, R.; Spoel, D.v.d.; Weckert, E.; Hajdu, J. *Nature* **2000**, *406*, 752-757.

(33) Barty, A.; Caleman, C.; Aquila, A.; Timneanu, N.; Lomb, L.; White, T.A.; Andreasson, J.; Arnlund, D.; Bajt, S.; Barends, T.R.M. et al. *Nature Photonics* **2012**, *6,* 35–40.

(34) Jurek, Z.; Faigel, G., *Europhys. Lett.* **2009**, *86*, 68003.

(35) Caleman, C.; Huldt, G.; Maia, F.R.N.C.; Ortiz, C.; Parak, F.G.; Hajdu, J.; Spoel, D.; Chapman, H.N.; Timneanu, N. *ACS Nano* **2011**, *5*, 139–146.

(36) Barty, A.; Boutet, S.; Bogan, M.J.; Hau-Riege, S.; Marchesini, S.; Sokolowski-Tinten, K.; Stojanovic, N.; Tobey, R.; Ehrke, H.; Cavalleri, A. et al., *Nat. Photon.* **2008**, *2*, 415–419.

(37) Popmintchev, T.; Chen, M.-C.; Popmintchev, D.; Arpin, P.; Brown, S.; Ališauskas, S.; Andriukaitis, G.; Balčiunas, T.; Mücke, O.D.; Pugzlys, A.; et al., *Science* **2012**, *336*, 1287.

(38) Berrah, N.; Bozek, J.; Costello, J.T.; Düstererd, S.; Fang, L.; Feldhaus, J.; Fukuzawa, H.; Hoener, M.; Jiang, Y.H.; Johnsson, P. et al. *Journal of Modern Optics, Topical Review* **2010**, *57* (12), 1015-1040.

(39) Rudenko, A.; Ullrich, J.; Moshammer, R. *Annu. Rev. Phys. Chem.*, **2012**, *63*, 635.

(40) Redecke, L.; Nass, K.; DePonte, D.P.; White, T.A.; Rehders, D.; Barty, A.; Stellato, F.; Liang, M.; Barends, T.R.M.; Boutet, S. et al., *Science* **2013**, *339*, 227–230.

(41) Boutet, S. et al., *Science* **2012**, *20*, 362–364.

(42) Chapman, H.N.; Fromme, P.; Barty, A.; White, T.A.; Kirian, R.A.; Aquila, A.; Hunter, M.S.; Schulz, J.; DePonte, D.P.; Weierstall, U. et al., *Nature* **2011**, *470*, 73–77.

(43) Seibert, M.M.; Ekeberg, T.; Maia, F.R.N.C.; Svenda, M.; Andreasson, J.; Jönsson, O.; Odić, D.; Iwan, B.; Rocker, A.; Westphal. D. et al., *Nature (London)* **2011**, *470*, 78-81.

(44) Owen, R.L.; Rudiño-Piñera, E.; Garman, E.F. *Proc. Natl. Acad. Sci.* **2006**, *103*, 4912 - 4917.

(45) Lomb, L.; Barends, T.R.M.; Kassemeyer, S.; Aquila, A.; Epp, S.W.; Erk, B.; Foucar, L.; Hartmann, R.; Rudek, B.; Rolles, D. et al., *Phys. Rev. B* **2011**, *84*, 214111.

(46) Johansson, O.; Bohl, E.; Henderson, G.G.; Mignolet, B.; Dennis, T.J.S.; Remacle, F,; Campbell, E.E.B. *J. Chem. Phys.* **2013**, *139*, 084309.

(47) Bozek, J. D. *Eur. Phys. J. Special Topics* **2009**, *169*, 129.

(48) Pešić, Z.D.; Rolles, D.; Perri, M.; Bilodeau, R.C.; Ackerman, G.D.; Rude, B.S.; Kilcoyne, A.L.D.; Bozek, J.D.; Berrah, N. *J. Elec. Spect. and Rel. Phen.* **2007**, *155*, 155.

(49) Bartels, R.; Backus, S.; Zeek, E.; Misoguti, L.; Vdovin, G.; Christov, I.P.; Murnane, M.M.; Kapteyn, H.C.; *Nature* **2000**, *406*, 164–166.

(50) Atomic Data and Nuclear Data Tables **1993**, *54*, 181-342.

(51) Kornilov, O. ; et al. J. Phys. B: At. Mol. Opt. Phys. 46 (2013) 164028

(52) Chemical Physics Letters 430 (2006) 167–172 (Hui)

(53) Wolf M. et al, Angew. Chem. Int. Ed. 2005, 44, 3306 –3309).

(54) Yang S. et al., J. AM. CHEM. SOC. 2006, 128, 16733).

(55) Zhang Y. et al., Nanoscale, 2014, 6, 11431

(56) Zewail, A. H.; *Angew. Chem. Int. Ed. Engl*, **2000**, *39*, 2586.

(57) Sansone, G.; Kelkensberg, F.; Morales, F.; Perez-Torres, J.F.; Martín, F. ;Vrakking, M.J.J. *IEEE, J. of Selec. topics in quantum electronics*, **2012**, *18*, 520.

(58) Petrovic, V.; et al. (Submitted to *Nat. Comm.*)

(59) Glownia, J.M.; Cryan, J.; Andreasson, J.; Belkacem, A.; Berrah, N.; Blaga, C.I.; Bostedt, C.; Bozek, J.; DiMauro, L.F.; Fang, L. et al. *Optics Express* **2010,** *18* (17), 17620-17630.

(60) Schnorr, K.; Senftleben, A.; Kurka, M.; A. Rudenko, A.; Foucar, L.; Schmid, G.; A. Broska, A.; T. Pfeifer,T.; K. Meyer,K.; Anielski,D.; et al., Phys. Rev. Lett. **2013**, 111, 093402.

(61) Castagna, J. C.; Murphy, B.; Bozek, J.; Berrah, N. *J. of Phys., Conference Series* **2013**, *425,* 152021.

(62) Yumoto, H.; Mimura, H.; Koyama, T.; Matsuyama, S.; Tono, K.; Togashi, T.; Inubushi, Y.; Sato, T.; Tanaka, T.; Kimura, T. et al., *Nat. Photon.* **2013**, *7*, 43 - 47.

(63) Osipov, T.; et al. *Bull. Am. Phys. Soc.* 134, (5), 87 Atlanta, Georgia, June 14th ,(2011).

(64) Ding, Y.; Brachmann, A.; Decker, F.-J.; Dowell, D.; Emma, P.; Frisch, J.; Gilevich, S.; Hays, G.; Hering, Ph.; Huang. Z. et al. *Phys. Rev. Lett.* **2009**, *102*, 254801.

(65) Amann, J.; Berg, W.; Blank, V.; Decker, F.-J.; Ding, Y.; Emma, P.; Feng, Y.; Frisch, J.; Fritz, D.; Hastings. J. et al., *Nat. Photon.* **2012**, *6*, 693-698.

(66) Wöstmann, M.; Mitzner, R.; Noll, T.; Roling, S.; Siemer, B.; Siewert, F.; Eppenhoff, S.; Wahlert, F.; Zacharias, H. *J. Phys. B* **2013**, *46*, 164005.

(67) Berrah, N.; Fang, L. *J. Elect. Spectros. And Relat. Phenom.,* submitted for publication, 2015.